City, University of London Institutional Repository

This is the accepted version of the paper.

This version of the publication may differ from the final published version.

Metal nanowire assisted hollow core fiber sensor for an efficient detection of small refractive index change of measurand liquid

A. K. Pathak*[a], S. Ghosh[b], R. K. Gangwar [c], B. M. A. Rahman[b], and V. K. Singh[a]

[a] Optical Fiber Laboratory, Indian Institute of Technology (Indian School of Mines), Dhanbad, Jharkhand, India.
[b] Department of School of Mathematics, Computer Science and Engineering, City University London, U.K.
[c] Centre for Applied Photonics, The Institute for Systems and Computer Engineering, Technology and Science (INESC-TEC) Porto, Portugal.
Email Id: akhileshpathak57@ap.ism.ac.in*[a], souvik.ghosh.1@city.ac.uk, rahul0889@gmail.com, b.m.a.rahman@city.ac.uk, vksingh@iitism.ac.in

Abstract

In this article, a cost-effective hollow core fiber (HCF) based refractive index (RI) sensor using surface plasmon resonance (SPR) is designed and demonstrated. The sensor consists of a metal nanowire inside an HCF along with the sensing medium of various refractive indices. SPR effect between polaritons and the guided core mode of designed HCF is exploited to enhance the sensing performance. A full vectorial finite element method (FEM) is used for the design and analyses of the sensing probes which exhibit very high sensitivities of 12400 nm/RIU, 10560 nm/RIU, and 6400 nm/RIU for Copper (Cu), Gold (Au), and Silver (Ag), respectively with a resolution of 1.61×10^{-6} RIU. Additionally, the influence of metal wire dimension is also investigated in this paper. The reported simple and low-cost sensor exhibits high sensitivity for liquid with refractive indices slightly higher than that of the dielectric tube, such as olive oil, turpentine, kerosene, chloroform, carbon tetrachloride, glycerol, Toluene etc.

Keywords

hollow core fiber; refractive index sensor; surface plasmon resonance; nanowire; sensitivity

Introduction

Since 1970, the optical fiber based RI sensors have been investigated and realized by researchers in the context of label-free detection of biochemical materials in liquids due to their small size, real-time detection, remote sensing capability and immunity to electromagnetic interference. Such sensors have numerous applications in environmental monitoring, chemical and biomedical and beyond. Various RI sensors have been designed and demonstrated relying e.g. photonic crystal fiber (PCF) [1], long period gratings, fiber Bragg grating [2], and tapered fiber [3], [4]. Most of researchers remove cladding partially or completely and the stripped section can also be coated with metal to enhance their sensitivity [5]. The stripping of cladding may enhance their sensitivity but make them more fragile for their practical use which may affect continuous monitoring. On the other hand, a PCF overcomes these limitations due to its flexible design, high confinement, and controllable birefringence. Moreover, the presence of air holes in PCF provides the opportunity to fill these holes with liquid and functional material which can effectively tune the effective refractive index (n_{eff}) of the core mode.

Several kind of RI sensor based on PCF using SPR technique have been reported [6]–[8]. In 2016, Wang *et al.* proposed PCF-SPR biosensor using silver-graphene layer [9] containing two types of air holes of different sizes while the central channel is filled with analyte which was coated with Ag and graphene layer. Wang realized an average sensitivity of 4350 nm/RIU for analytes (n_a) range between 1.39-1.42 and selectively coated sensor enhanced the sensitivity due to large surface to volume ratio. Later in 2018 Liu et al. also proposed a liquid infiltrated Au coated SPR based RI sensor in which the air holes are arranged in a square lattice [10] and the maximum sensitivity of 6300 nm/RIU was reported. These sensors, although have provided a higher sensitivity, but still they suffered complexity in realization like designing and metal coating. To overcome these limitations researchers attracted towards the metal nanowire instead of coating which is easy to place and also cost-effective. In this regard, Liu et al. demonstrated a SPR based RI sensor with selectively filled liquid inside the PCF air holes and realized the maximum sensitivity of 2350 nm/RIU for low refractive index ranges between 1.27 to 1.36 [11]. The designed sensor consists a large microfluidic channel which may help to avoid channel interference with each

---

* Corresponding author

other. Recently, Swillam *et al.* demonstrated a highly sensitive SPR based biosensor using nanorod and achieve a high sensitivity of 7900 nm/RIU [12]. In these cases, the plasmonic modes are formed on nanowire and thus excite localized surface plasmon resonance (LSPR) due to phase matching of SPP and core guided modes [13], [14]. The present work is inspired by previously reported article by Luan and Yao in which they developed a hollow fiber RI sensor for a high RI analyte using silver nanowire to achieve high sensitivity [15]. Our work considers the similar sensor design to analyze its performance but with different metallic nanowires to study their sensing performances for lower RI medium.

In this paper, we have considered a SPR based hollow core fiber refractive index (HCFRI) sensor selectively filled with analytes and metal nanowire. The investigation is carried out for three different metallic nanowires, Au, Ag and Cu to evaluate their sensing performances. Numerically simulated results illustrate that sensor containing Cu nanowire exhibits a higher sensitivity in comparison to Ag and Au nanowires. The proposed sensor is designed and optimized by using COMSOL Multiphysics [16] based on vectorial finite element method (FEM) and consider the confinement losses, sensitivity and coupling length. The designed sensor is examined for a wide range of RI varying between 1.46-1.48 and a high sensitivity of 12560 nm/RIU is obtained with sensor filled with Cu nanowire which is higher than previously reported articles [12], [17], [18].

Design and theoretical modeling

The schematic cross-section view of the designed HCFRI sensor is shown in Fig.1. The diameter of the fiber, its hollow core, and Cu nanowire are defined as D, d_s and d_n, respectively. As shown here liquid and Cu nanowire are infiltrated in the hollow section of fiber. The Cu nanowire sinks to the bottom of liquid filled hollow core due to gravity effect and rests at the bottom [19]. The background material of fiber can be made of silica glass of RI=1.45. The refractive index of Cu is calculated by using Lorentz-Drude model [20]. The designed sensor is characterized by COMSOL Multiphysics software which is based on full-vectorial finite element method [21]. Here, a very fine mesh has been used in which the whole sensor cross-section is divided in many triangular subdomains. All the modal analyses are performed in the XY plane and light is considered to propagate in the Z-direction.
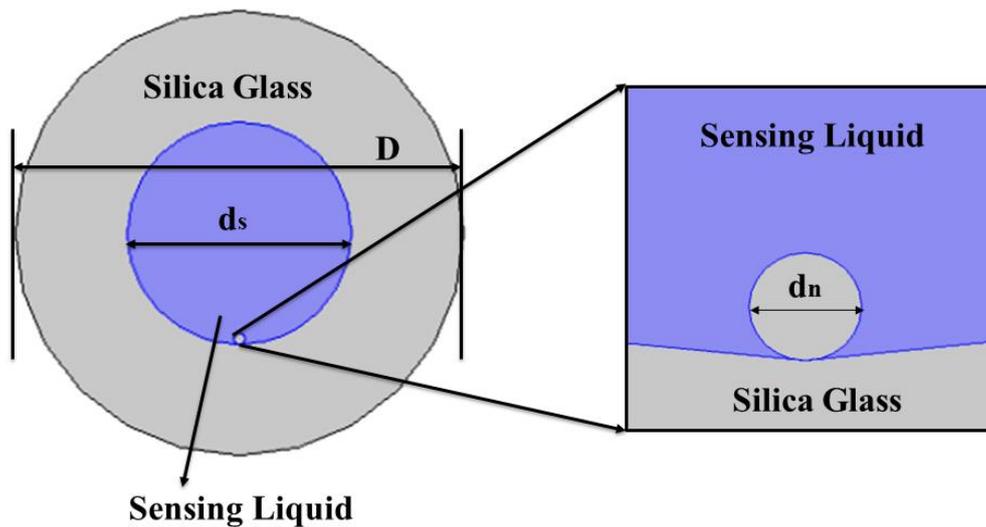

Fig.1. Schematic diagram of the designed HCFRI sensor.

The experimental realization of proposed sensor is also possible. The setup will contain a broadband source (BBS), optical spectrum analyzer (OSA) and designed sensor. Initially, the liquid and nanowire are filled in HCF, then both end of designed HCF sensor are spliced to single mode fibers (SMFs) using fusion splicer. In the experimental work the transmission spectrum at various RI and their shifting can be used to determine the wavelength sensitivity of designed sensor.

* Corresponding author

Result and discussions

The designed HCFRI sensor is based on simple SPR technique between surface plasmon polaritons (SPP) and core-guided mode. It is mainly occurring due to the enhanced evanescent waves and their direct interaction with analytes (n_a) of varying RI. The evanescent waves easily excite the free electron available on the surface of a Cu nanowire at a particular wavelength, which is known as plasmon resonance wavelength (λ_R). At this λ_R the free electron of nanowire generates the surface plasmon waves.

The modal loss of the designed sensor is calculated from the imaginary part of effective index by following relation [22]

$$\alpha(dB/m) = 8.686. \, k_0. \, Im \, (n_{eff}) \qquad (1)$$

where the wavenumber $k_0 = 2\pi/\lambda$.

Here, variations of real effective index ($Re(n_{eff})$) of both core and SPP modes and the modal loss with the wavelength for the diameters, $D = 40 \, \mu m$, $d_s = 20 \, \mu m$, $d_n = 0.55 \, \mu m$ and $n_a = 1.46$ are shown in Fig.2. The effective index of core mode is nearly constant with the operating wavelength, shown here by a black line with black circles. On the other hand, the effective index of highly dispersive plasmonic mode along the metal wire reduces rapidly with the wavelength as shown by a blue line with blue circles. The dielectric core mode is not lossy but the plasmonic mode is highly lossy. When these two effective indices intersect (actually anticrossing points) then due to interaction between core mode and highly lossy plasmonic mode, modal loss of this core dielectric core mode increases rapidly, which is shown by black line with red circles. A sharp peak at phase-matching wavelength, λ_R = 1.615 μm with maximum loss of 13.66 dB/mm can be observed. This demonstrates that at this λ_R maximum power get transferred from low loss core mode to a very lossy SPP mode.
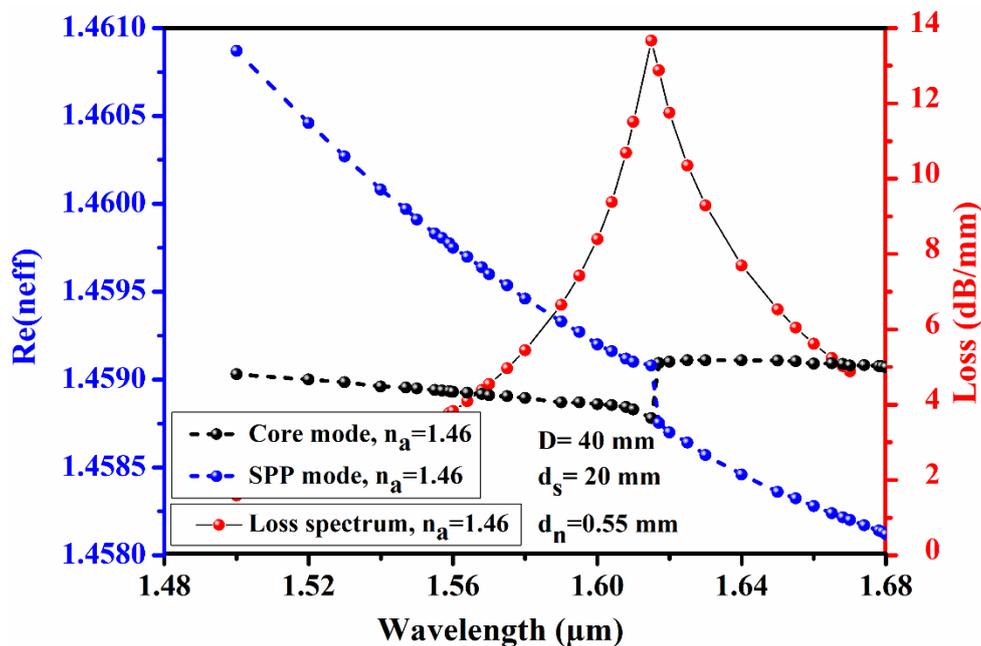

Fig.2. Dispersion relation between core mode and SPP mode.

Figure 3 shows the H_x field contour and their corresponding H_x field variation along the y-axis for the core mode and SPP mode at λ_R =1.5 μm with n_a = 1.46. The H_x contour profile for the plasmonic mode is shown on the left of Fig. 3(b). It can be observed that this mode is localized around the metal nanowire. Its variation along the y-axis is shown on the right, which clearly shows plasmonic peak at the metal-dielectric interfaces and the decay exponentially. While Fig. 3(a) illustrates the mode coupling of core guided mode with the SPP mode. The

* Corresponding author

moderate H_x field value in the core is clearly shown, but a more localized H_x field around the nanowire is also visible. Its variation along the y-axis is shown on the right which is clearly shows the coupled supermode profile along the y-axis.
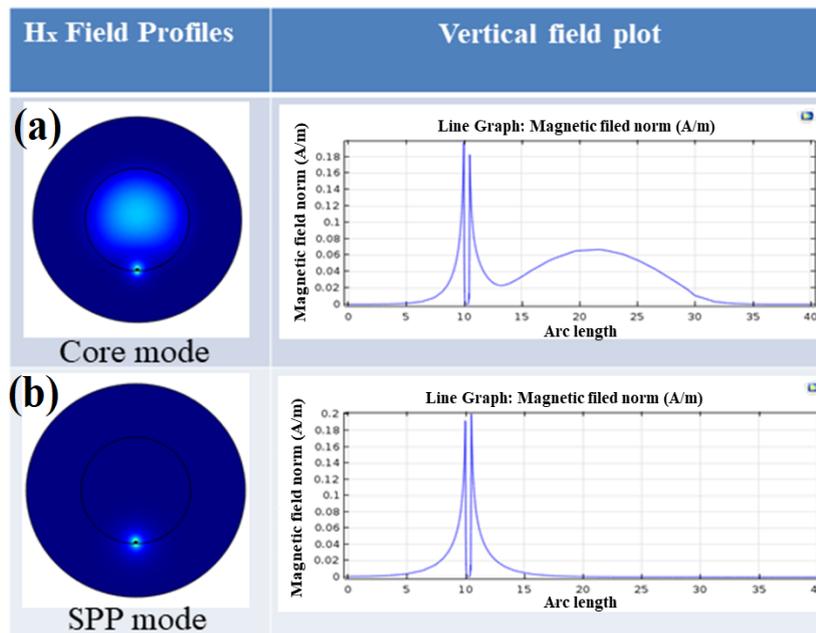

Fig.3. H_x profiles for core mode and SPP mode at λ=1.5 µm.

At first, we investigate the sensing performance of different nanowires like Ag, Au, and Cu to select the best metal to design highly sensitive RI sensor. Figure 4 exhibits the modal loss spectra for Cu nanowire at diameter 0.55 µm. Variation of modal loss with the wavelength for n_a=1.46 is shown by solid black line. It can be observed that the loss value reaches to 13.66 dB/mm at λ=1.615 µm. However, when the RI changes from n_a=1.46 to n_a=1.47 the modal loss peak shifted from λ =1.615 µm to λ=1.46 µm, shown by solid red line. From Fig. 4 we can clearly see a large wavelength shift of △λ =0.15 µm, while n_a changes from 1.46 to 1.47.
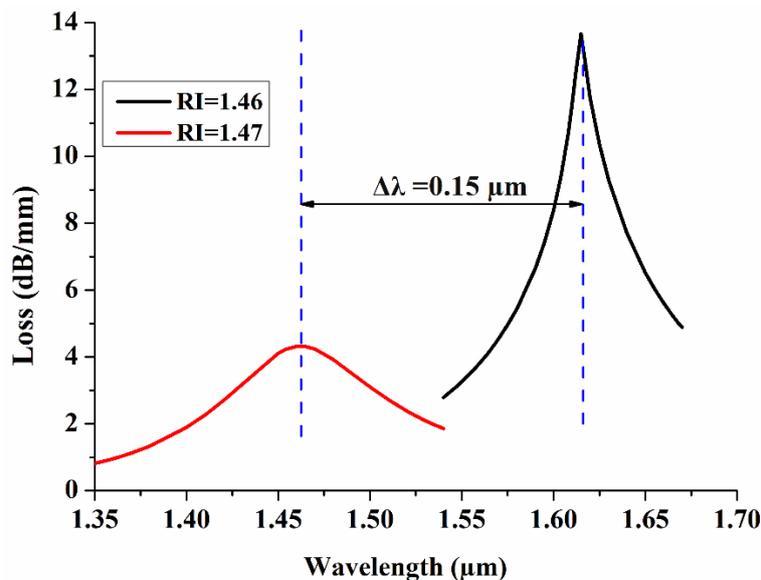

Fig.4. Confinement loss spectra at n_a=1.46 as a function of wavelength for Cu nanowire (d_n =0.55 µm).

* Corresponding author

Figures 5 and 6 exhibit the modal loss spectra variations with respect to wavelength for Au and Ag nanowire, respectively. In Figs. 5 and 6 we can clearly identify the modal loss of 11.78 dB/mm and 9.36 dB/mm at λ=1.545 and λ=1.195 for Au and Ag, respectively at n_a=1.46, which is comparatively less than that of the Cu nanowire. While we have changed n_a from 1.46 to 1.47 the modal loss of Au and Ag shifted to λ=1.415 and λ=1.115, respectively. These analyses are carried out with their optimized diameter. Moreover, these figures also illustrate a smaller wavelength shift of $\triangle\lambda$ =0.13 and $\triangle\lambda$ =0.08, for Au and Ag, respectively which is comparatively less than, Cu nanowire. Hence throughout the analysis, we clearly observe that Cu nanowire gives a large wavelength shift and the larger wavelength shift is expected to show high wavelength sensitivity, which is the basic reason that we have carried out further analysis with Cu nanowire.
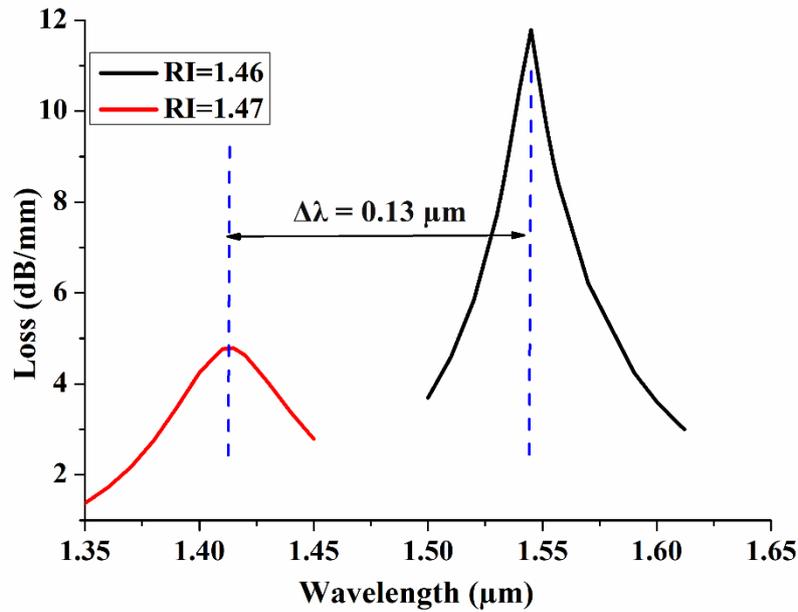

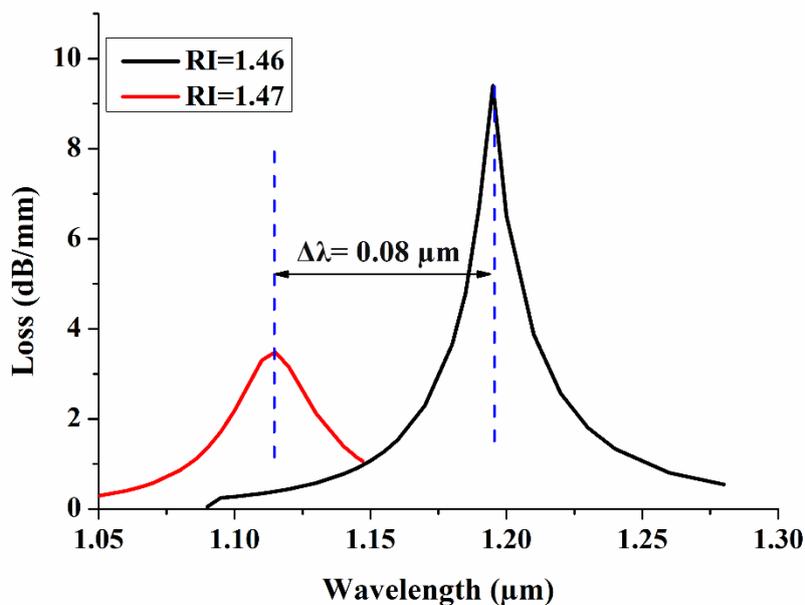**Fig. 5**. Confinement loss spectra at n_a=1.46 as a function of wavelength for Au nanowire (d_n =0.45 µm).

Fig. 6. Confinement loss spectra at n_a=1.46 as a function of wavelength for Ag nanowire (d_n =0.25 µm).

The diameter of nanowire (d_n) also shows a considerable influence on sensing performance [23]. So, we must optimize the diameter of nanowire before they can be used in sensing applications. Variations of modal loss

* Corresponding author

spectra with the wavelength for different d_n are shown in Fig. 7. Here, we have taken three different metal nanowire diameters, d_n of 0.5 μm, 0.55 μm and 0.6 μm in which the nature of loss spectra is clearly observed. The maximum loss of 13.66 dB/mm is obtained for $d_n = 0.55$ μm while 12.80 dB/mm and 12.82 dB/mm is obtained for $d_n = 0.50$ μm and 0.6 μm, respectively. Next, effect of nanowire diameter on peak loss value is studied. Figure 8 clearly shows that initially the maximum confinement loss starts increasing up to the diameter $d_n = 0.55$ μm and then start decreasing gradually, due to a strong coupling between loss core mode and the SPP mode at $d_n = 0.55$ μm. The increase in d_n results the redshift of peak wavelength due to the increase in n_{eff} of SPP mode. Hence, we have obtained a maximum loss for $d_n = 0.55$ μm which can be used as the optimized diameter.
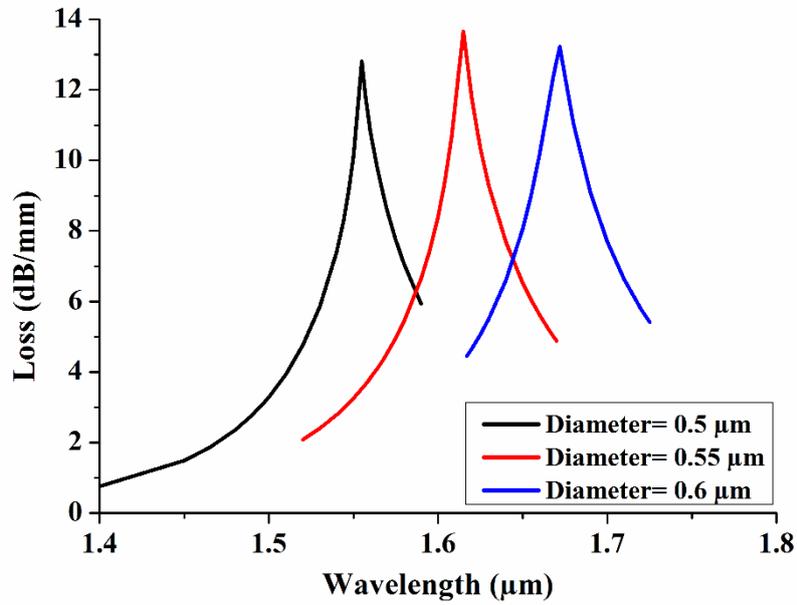

Fig.7. The confinement loss spectra of designed sensor when d_n changes from 0.5 μm to 0.6 μm.

Fig. 8. Influence of diameter (d_n) variation on the sensitivity.

Next, we have investigated the sensor response for various RI value of n_a is varying between 1.46 to 1.48. Since the n_{eff} of the SPP mode strongly depends on the RI of surrounding media, hence the small change in RI leads the change in n_{eff} of SPP mode and hence in resonance shift λ_R. The confinement loss for each RI is calculated by Eq.

* Corresponding author

(1). Figure 9 shows the nature of dispersion relation between core mode and SPP mode at different n_a. We may clearly observe the blue shifting in dispersion curves for different n_a varying from 1.46-1.48. At n_a =1.46, the core guided mode shown by black dotted line intersect with SPP mode shown by red dotted line which illustrate the phase matching point with λ_R= 1.615 µm. As the core index n_a increases, the effective index increases shown by two horizontal lines. So, their phase matching points are shifted towards the lower wavelength with λ_R = 1.45 and λ_R = 1.34, for analyte index, 1.47 and 1.48, respectively.
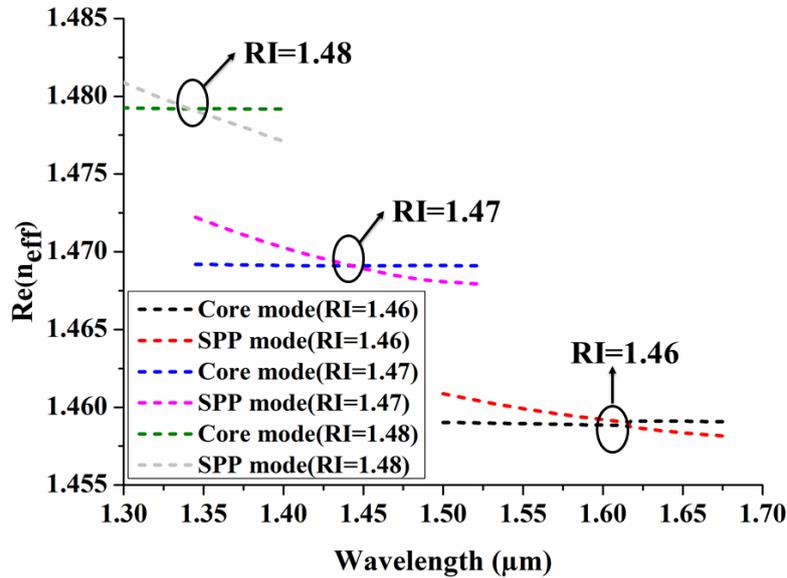

Fig.9. Dispersion relation between core mode and plasmonic mode for different RI.

In Fig.10 we can clearly see that with increase in RI of surrounding media, the λ_R is shifted towards the lower wavelength i.e. the blue shift in loss spectra appears with gradually decreasing peak loss. When the n_a of surrounding changes from 1.46, 1.465, 1.47, 1.475 and 1.48 the loss spectra shifted with maximum confinement loss of 13.66 dB/mm, 6.42 dB/mm, 4.32 dB/mm, 3.21 dB/mm and 2.52 dB/mm, respectively. With increase in RI of analytes, the n_{eff} of SPP mode reach closer to n_{eff} of core guided mode and hence the energy transfer gets increases from core mode to SPP mode and leads the maximum confinement loss.
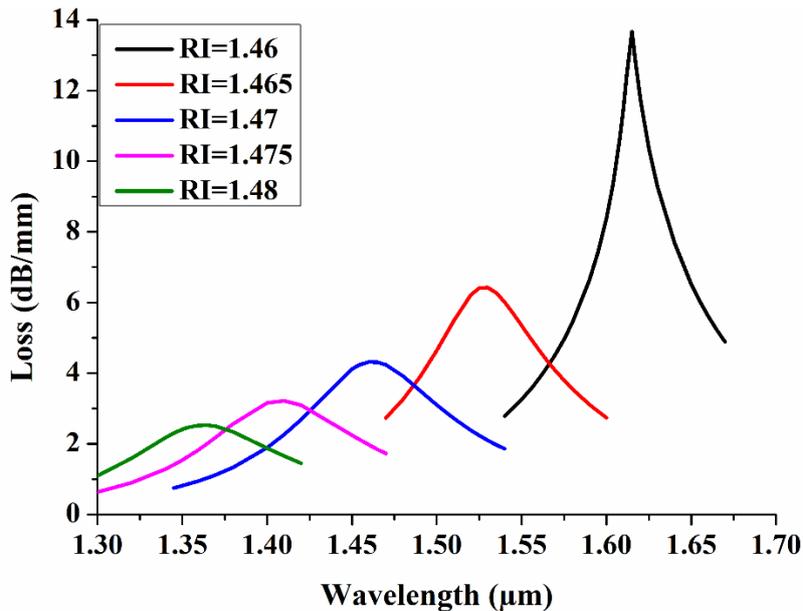

Fig.10. Confinement loss spectra with various RI.

* Corresponding author

The coupling length may define as the length at which the complete power transfer from one mode to another mode takes place and it can be calculated by following equation [24]

$$L_c = (\pi / \Delta\beta) \qquad (2)$$

where L_c represent the coupling length and $\Delta\beta$ shows the difference of propagation constants between these two modes. Figure 11 shows the coupling length corresponding to $n_a = 1.46$, 1.47 and 1.48 denoted shown by blue, red and black dotted lines, respectively. It can be also noted that for a larger n_a value, the higher intersecting angle reduces the separation at the anticrossing point so peak L_c increases.

Fig.11. Coupling length corresponding to given RI.

The performance of designed HCFRI sensor is investigated in term of their sensitivity, linearity, and resolution. The relationship between resonance wavelength and corresponding RI is illustrated in Fig. 12. From this figure, we can clearly observe a good linear response between resonance wavelength and n_a with $R^2 = 0.97$ for the varying range of 1.46 to 1.48.

Fig.12. Sensitivity plot for designed sensor.

* Corresponding author

The sensitivity of designed sensor is calculated by using the following relation, [25]-
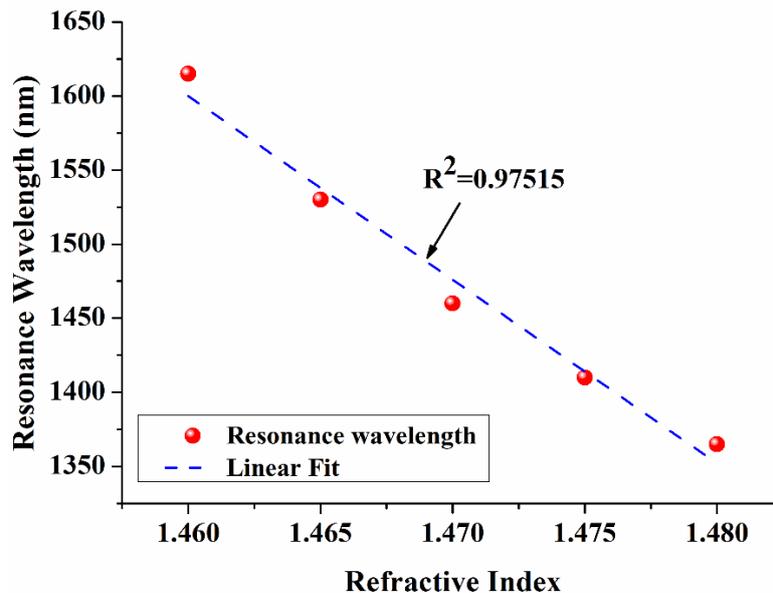
$$S_\lambda = \Delta\lambda_{peak}/\Delta n_a \text{ (nm/RIU)} \quad (3)$$

where, $\Delta\lambda_{peak}$ represent the change in resonance wavelength peak and Δn_a represent the change in surrounding analytes. The proposed sensor clearly exhibits a very high sensitivity of 12400 nm/RIU for RI varying between 1.46 to 1.48 with $d_n = 0.55$ μm. We have also calculated the sensitivity for other metal nanowires such as, Au and Ag to study the influence of metal on the sensitivity. Figure 13 illustrates the relationship between resonance wavelength and RI for various nanowires.
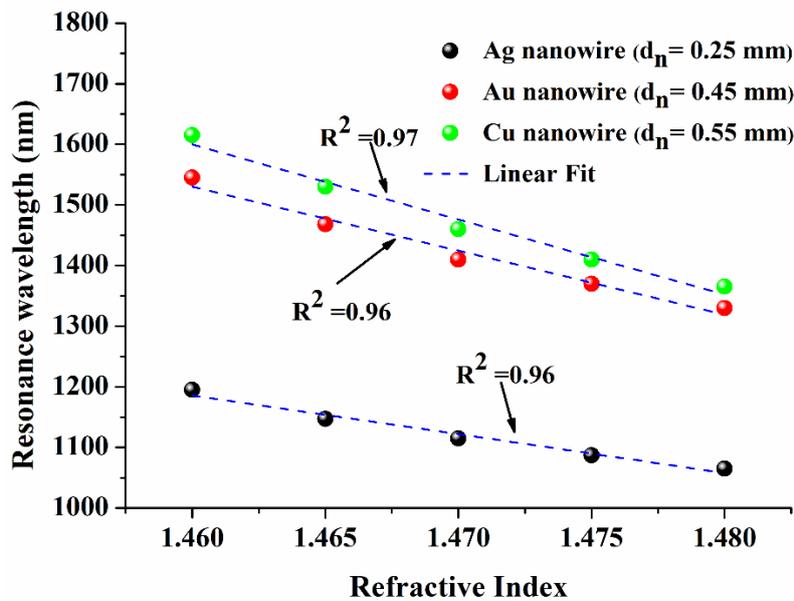

Fig.13. Relationship between resonance wavelength and RI for different d_n.

Table I shows the sensitivity values obtained for Au, Ag and Cu nanowires.

TABLE I
Sensitivity comparison of different metal nanowires

Nanowire	Sensitivity(nm/RIU)
Cu	12400
Au	10560
Ag	6400

The resolution of designed HCFRI sensor can be calculated by following equation-

$$R = \Delta n_a \times (\Delta\lambda_{min}/\Delta\lambda_{peak}) \text{ RIU} \quad (4)$$

where, $\Delta\lambda_{min}$ represent the minimum change in spectral resolution and $\Delta\lambda_{peak}$ represent the change in peak wavelength. If we consider 0.02 nm as the minimum spectral resolution [26] then the resolution of our designed sensor is 1.61×10^{-6} RIU. The resolution of our sensor express that our sensor is capable to measure small variation in analytes in the order 10^{-6}. Thus, we can state that our designed sensor is can be used effectively in small range too. From the obtained results we can also state that Ag nanowire designed here can provide high sensitivity compared to the previous results [15]. However, our result states that Cu gives highest sensitivity for low RI range varying from 1.46-1.48. Result shown in Table I also provide the evidence that we may avoid use of Cu and Ag in case of oxidation [27] and can choose Au for higher sensitivity and greater stability than other metals.

* Corresponding author

Conclusion

In conclusion, we have designed and demonstrated an HCFRI sensor based on SPR technique and analyzed by using COMSOL Multiphysics. The sensor assisted with Cu nanowire not only just reduces its cost but also provide a high sensitivity of 12400 nm/RIU in comparison to other more expensive metal like Ag and Au. A wide range of RI is analyzed in present work varying between $n_a = 1.46$-1.48. The sensing responses are analyzed in term of their sensitivity, resolution, and linearity. From the obtained results we can say that our designed HCFRI sensor will be promising in development of highly sensitive and cost-effective RI sensor. However, for a given range of sensing media, the diameter of metal wire needs to be optimized to obtain its peak sensitivity in the available range of a wavelength source. These values are intricately related and sensor parameters need to be optimized for a given application. It will be useful in measuring the RI of many household materials like olive oil, kerosene and coconut oil and some chemicals like chloroform, ethylene glycol, polylactic acid, glycerol, etc.

Acknowledgment

References

[1]   R. K. Gangwar and V. K. Singh, "Refractive index sensor based on selectively liquid infiltrated dual core photonic crystal fibers," Photonics Nanostructures - Fundam. Appl., vol. **15**, pp. 46–52, Jun. 201

[2]   Y. Miao, B. Liu, and Q. Zhao, "Refractive index sensor based on measuring the transmission power of tilted fiber Bragg grating," Opt. Fiber Technol., vol. **15**, no. 3, pp. 233–236, Jun. 2009.

[3]   C. Chen, R. Yang, X. Zhang, W. Wei, Q. Guo, X. Zhang, L. Qin, Y. Ning, and Y. Yu, "Compact refractive index sensor based on an S-tapered fiber probe," Opt. Mater. Express, vol. **8**, no. 4, pp. 919-925, Apr. 2018

[4]   P. Lu, J. Harris, X. Wang, G. Lin, L. Chen, and X. Bao, "Tapered-fiber-based refractive index sensor at an air/solution interface," Appl. Opt., vol. **51**, no. 30, pp. 7368-7373, Oct. 2012.

[5]   A. K. Mishra, S. K. Mishra, and B. D. Gupta, "SPR based fiber optic sensor for refractive index sensing with enhanced detection accuracy and figure of merit in visible region," Opt. Commun., vol. **344**, pp. 86–91, Jun. 2015.

[6]   Z. Liu, X. Yang, Y. Zhang, Y. Zhang, Z. Zhu, X. Yang, J. Zhang, J. Yang, and L. Yuan, "Hollow fiber SPR sensor available for microfluidic chip," Sens. Actuator B-Chem., vol. **265**, pp. 211–216, Jul. 2018.

[7]   X. Li, L. V. Nguyen, Y. Zhao, H. Ebendorff-Heidepriem, and S. C. Warren-Smith, "High-sensitivity Sagnac-interferometer biosensor based on exposed core microstructured optical fiber," Sens. Actuator B-Chem., vol. **269**, pp. 103–109, Sep. 2018.

[8]   Z. Liu, H.-Y. Tam, L. Htein, M.-L. V. Tse, and C. Lu, "Microstructured Optical Fiber Sensors," J. Light. Technol., vol. **35**, no. 16, pp. 3425–3439, Aug. 2017.

[9]   F. Wang, Z. Sun, C. Liu, T. Sun, and P. K. Chu, "A highly sensitive dual-core photonic crystal fiber based on a surface plasmon resonance biosensor with silver-graphene layer," Plasmonics, vol. **12**, no. 6, pp. 1847–1853, Dec. 2017.

[10]   C. Liu, W. Su, F. Wang, X. Li, Q. Liu, H. Mu, T. Sun, P. K. Chu, and B. Liu, "Birefringent PCF based SPR sensor for a broad range of low refractive index detection," IEEE Photonics Technol. Lett., vol. **30**, pp. 1471 - 1474, Jul. 2018.

[11]   C. Liu, L. Yang, Q. Liu, F. Wang, Z. Sun, T. Sun, H. Mu, and P. K. Chu, "Analysis of a surface plasmon resonance probe based on photonic crystal fibers for low refractive index detection," Plasmonics, vol. **13**, no. 3, pp. 779–784, Jun. 2018.

[12]   M. Y. Azab, M. A. Swillam, M. Farahat, A. Heikal, and S. A. A. Obayya, "Analysis of highly sensitive surface plasmon photonic crystal fiber biosensor," in Photonic and Phononic Properties of Engineered Nanostructures VIII-SPIE, vol. **10541**, 2018, pp. 58.

[13]   H. W. Lee, M. A. Schmidt, H. K. Tyagi, L. P. Sempere, and P. St. J. Russell, "Polarization-dependent coupling to plasmon modes on submicron gold wire in photonic crystal fiber," Appl. Phys. Lett., vol. **93**, no. 11, pp. 111102, Sep. 2008.

[14]   A. Csaki, F. Jahn, I. Latka, T. Henkel, D. Malsch, T. Schneider, K. Schröder, K. Schuster, A . Schwuchow,

* Corresponding author

R. Spittel, D. Zopf, and W Fritzsche , "Nanoparticle layer deposition for plasmonic tuning of microstructured optical fibers," Small, vol. **6**, no. 22, pp. 2584–2589, Nov. 2010.

[15] N. Luan and J. Yao, "High Refractive Index Surface Plasmon Resonance Sensor Based on a Silver Wire Filled Hollow Fiber," IEEE Photonics J., vol. **8**, no. 1, pp. 1–9, Feb. 2016.

[16] "COMSOL Multiphysics® Modeling Software." [Online]. Available: https://www.comsol.com/.

[17] G. An, X. Hao, S. Li, X. Yan, and X. Zhang, "D-shaped photonic crystal fiber refractive index sensor based on surface plasmon resonance," Appl. Opt., vol. **56**, no. 24, pp. 6988-6992, Aug. 2017.

[18] J. N. Dash, R. Das, and R. Jha, "AZO Coated Microchannel incorporated PCF-based SPR sensor: A numerical analysis," IEEE Photonics Technol. Lett., vol. **30**, no. 11, pp. 1032–1035, Jun. 2018.

[19] X. Yang, Y. Lu, L. Duan, B. Liu, and J. Yao, "Temperature sensor based on hollow fiber filled with graphene-Ag composite nanowire and liquid," Plasmonics, vol. **12**, no. 6, pp. 1805–1811, Dec. 2017

[20] A. D. Rakić, A. B. Djurišić, J. M. Elazar, and M. L. Majewski, "Optical properties of metallic films for vertical-cavity optoelectronic devices," Appl. Opt., vol. **37**, no. 22, pp. 5271-5283, Aug. 1998.

[21] B. M. A. Rahman and J. B. Davies, "Finite-element analysis of optical and microwave waveguide problems," IEEE Trans. Microw. Theory Tech., vol. **32**, no. 1, pp. 20–28, Jan. 1984.

[22] R. K. Gangwar and V. K. Singh, "Highly sensitive surface plasmon resonance based D-shaped photonic crystal fiber refractive index sensor," Plasmonics, vol. **12**, no. 5, pp. 1367–1372, Oct. 2017.

[23] Y. Lu., C. Hao, B. Wu, X. Huang, W. Wen, X. Fu, and J. Yao, "Grapefruit fiber filled with silver nanowires surface plasmon resonance sensor in aqueous environments," Sensors, vol. **12**, no. 9, pp. 12016–12025, Aug. 2012.

[24] H. Jiang, E. Wang, K. Xie, and Z. Hu, "Dual-core photonic crystal fiber for use in fiber filters," IEEE Photonics J., vol. **8**, no. 2, pp. 1–8, Apr. 2016.

[25] E. K. Akowuah, T. Gorman, H. Ademgil, S. Haxha, G. K. Robinson, and J. V. Oliver, "Numerical analysis of a photonic crystal fiber for biosensing applications," IEEE J. Quantum Electron., vol. **48**, no. 11, pp. 1403–1410, Nov. 2012.

[26] W. Zhang, Z. Lian, T. Benson, X. Wang, and S. Lou, "A refractive index sensor based on a D-shaped photonic crystal fiber with a nanoscale gold belt," Opt. Quantum Electron., vol. **50**, no. 1, pp. 29, Jan. 2018.

[27] S.-S. Chee and J.-H. Lee, "Preparation and oxidation behavior of Ag-coated Cu nanoparticles less than 20 nm in size," J. Mater. Chem. C, vol. **2**, no. 27, pp. 5372–5381, Jun. 2014.

* Corresponding author